Air-sea gas exchange measurements helped derive in-situ organic and inorganic carbon fixation in response to Ocean Alkalinity Enhancement in a temperate plankton community

Julieta Schneider[1], Ulf Riebesell[1], Charly A. Moras[2,3], Laura Marín-Samper[4], Leila R. Kittu[1], Joaquín
Ortíz-Cortes[1], Kai G. Schulz[2]

[1] GEOMAR Helmholtz Centre for Ocean Research Kiel, Wischhofstrasse 1-3, 24148 Kiel, Germany
[2] Faculty of Science and Engineering, Southern Cross University, Lismore, NSW, Australia
[3] Institute for Geology, Universität Hamburg, 20146, Hamburg, Germany
[4] Instituto de Oceanografía y Cambio Global, Universidad de Las Palmas de Gran Canaria, 35017 Telde, Spain

Correspondence to: Julieta Schneider (jschneider@geomar.de) and Kai G. Schulz (kai.schulz@scu.edu.au)

Abstract. Ocean Alkalinity Enhancement (OAE) is a carbon dioxide removal strategy that aims to chemically sequester atmospheric CO_2 in the ocean while potentially alleviating localized effects of ocean acidification. Depending on the implementation approach, OAE can considerably alter seawater carbonate chemistry, resulting in reduced CO_2 partial pressures (pCO_2) and high pH. To investigate the effects of OAE on biogeochemical processes and organisms under close-to-natural conditions, a large-scale mesocosm experiment was conducted in the temperate fjord ecosystem near Bergen, Norway during late spring. A non-CO_2-equilibrated approach was chosen, simulating OAE with calcium- and silicon-based minerals. A gradient of five OAE levels was achieved by increasing total alkalinity (TA) by 0-600 µmol kg^{-1}. The added TA remained relatively stable over the 47-day experimental period and the measured CO_2 gas exchange rate was comparable to what would be expected for large oceanic regions. We estimated that full equilibration (95%) for a ΔTA of 600 µmol kg^{-1} would take ~1050 days. Furthermore, there were a number of mineral-type and pCO_2/pH effects, with cumulative coccolithophore calcification showing an optimum curve response to decreasing pCO_2, consistent with findings from single-species laboratory cultures, while no mineral-type effect was observed. In contrast, *in-situ* net community production was higher in the silicate treatments but there was no pCO_2 effect. Zooplankton respiration, estimated from *in-situ* net community production and *in-vitro* net community production incubations, was lower for the silicate treatments and negatively correlated with pCO_2. These complex findings suggest both direct and indirect effects of mineral type and OAE level and provide a valuable foundation for designing future OAE field trials.

1 Introduction

The rapid increase in atmospheric carbon dioxide (CO_2) concentration over the last 250 years has been identified as a major cause for global warming, with current modelling projections for 2100 exceeding 2°C above pre-industrial levels (Peters, 2016; Rogelj et al., 2016). This is a critical threshold associated with the onset of extreme weather events (Schellnhuber et al., 2016). However, decreasing CO_2 emissions will not be sufficient to achieve a net-zero target towards the end of this century (Ho, 2023), which would be required to stay below the 2°C threshold (Rogelj et al., 2018). Therefore, it is paramount to explore the potential of active atmospheric CO_2 removal (CDR) strategies (IPCC, 2021; Van Vuuren et al., 2018). Ocean alkalinity enhancement (OAE) is a marine CDR approach with significant potential, that relies on speeding up the natural process of rock weathering via the addition of alkaline solutions/minerals. By adding alkaline feedstocks to seawater (Kheshgi, 1995), the subsequent increase in alkalinity and pH lowers surface water CO_2 concentrations, hence creating a CO_2 sink or reducing a CO_2 source if the water is naturally oversaturated (Caserini et al., 2021; Denman, 2008; Feng et al., 2016; Hartmann et al., 2013; Köhler et al., 2010; National Academies of Sciences, 2022; Sabine and Tanhua, 2010). The localized increase in total alkalinity (TA) and pH simultaneously mitigates ocean acidification (OA), even after eventual CO_2 equilibration with the atmosphere (Moras et al., 2022). Modelling studies suggest that the CO_2 uptake potential of OAE ranges between 14 and 41 gigatons per year (Oschlies et al., 2023). This variability underscores a significant knowledge gap between modelled predictions and real-world conditions, which needs to be acknowledged and addressed (Henderson et al., 2008).

There are two very distinct approaches to performing OAE additions: CO_2-equilibrated, which involves equilibrating the high TA seawater with atmospheric CO_2 prior to release, and non-CO_2-equilibrated, which relies on natural air-sea gas exchange to achieve equilibration over time. For the latter process to happen, it is crucial that the alkalized water remains in the surface ocean in contact with the atmosphere. Since gas exchange could take months to years (He and Tyka, 2023) and depend heavily on the degree of dilution of the high-TA water with the surrounding seawater, marine organisms might be exposed to CO_2 depleted conditions and relatively high pH levels, which could be detrimental to planktonic communities (Doney et al., 2020; Kroeker et al., 2010). However, experimental data on potential biological OAE effects are scarce (National Academies of Sciences, 2022), and thresholds of applicability not yet fully understood. For instance, recent studies have identified the potential risks of runaway calcium carbonate ($CaCO_3$) precipitation beyond certain pH thresholds which should be avoided since it reduces the CDR potential of OAE (Fuhr et al., 2022; Hartmann et al., 2023; Moras et al., 2022; Paul et al.,2024; Suitner et al., 2024).

A number of potentially suitable OAE feedstocks have been previously suggested (Hartmann et al., 2013; Renforth and Henderson, 2017), including quick or hydrated lime (calcium-based), brucite (magnesium-based), and olivine (silicate-based), all of which release soluble products of interest for marine organisms (Montserrat et al., 2017; Moras et al., 2024). For these materials, Bach et al., (2019) hypothesized that the increase in calcium ions (Ca^{+2}) together with DIC upon equilibration, would benefit the calcification process of key calcifiers such as coccolithophores, which are highly impacted by ocean acidification; while the release of $Si(OH)_4$ could benefit diatoms, another group of primary producers that rely on silicate to synthesize their exoskeletons. This hypothesis, termed "*white vs green ocean*" stresses the importance to assess the biological response of natural ecosystems to OAE with respect to the type and concentration of the alkaline material used.

This research presents the first data on the temporal dynamics of the carbonate system within large-scale mesocosms following deployment of silicon- and calcium-based OAE treatments ranging from 0 to 600 µmol kg^{-1} of added alkalinity. We conducted a 53-day *in situ* experiment using 10 pelagic mesocosms (Riebesell et al., 2013) in Bergen, Norway. OAE release was in a non-pre-equilibrated way, i.e., the ingassing of CO_2 was left to occur naturally via air-sea gas exchange, which is believed to represent the most feasible deployment scenario from both a technological and an economical

perspective (Schulz et al., 2023). However, this approach can also lead to strong perturbations of seawater carbonate chemistry, namely high pH, low partial pressure of seawater CO_2 (pCO_2), and high seawater aragonite saturation states (Ω_A). These perturbations would be highest close to an OAE point source prior to dilution and atmospheric CO_2 uptake.

75 Here, we focused on assessing OAE induced carbonate chemistry changes, the stability of alkalinity over time (including biogenic calcification), as well as deriving air-sea CO_2 exchange rates from measurements, allowing to also calculate net ecosystem primary productivity. Processes that need to be better understood before large field deployments of OAE and for later monitoring and verification.

2 Materials and Methods

80 ### 2.1 Mesocosm deployments and experimental setup

Ten Kiel Off-Shore Mesocosms for Future Ocean Simulations (KOSMOS) were deployed by the research vessel ALKOR and moored in the Raunefjord, Norway on the 7th of May 2022 (60.25N 5.2E). The technical design of these seagoing mesocosms and procedures for water column manipulation are described in detail by Riebesell et al (2013). Briefly, the 20 m long mesocosm bags were suspended in 8m tall floating frames and both ends were covered with a 3 mm mesh size

85 net to exclude larger organisms during filling. The tops of the bags were then submerged 1 meter below the sea surface and fully unfolded to enclose a waterbody containing the natural planktonic community. The bags were left submerged for 5 days to allow for sufficient seawater exchange to ensure similar starting conditions in all mesocosms. Next, the waterbody within the mesocosm bags was isolated from the surroundings by attaching a 2 m-long, funnel-shaped sediment trap on the lower end of the bags and lifting the top end 1m above the surface. The attachment of the sediment trap on the

90 13th of May marked the beginning (day 0) of the 53-day experiment. Right after closure, a 1mm net was pulled from bottom to top to remove any heterogeneously distributed nekton. From day 1 to 3, daily samplings were conducted to monitor the initial conditions of the enclosed waters before OAE manipulation on day 6. Additionally, a volume determination based on the salinity change after addition of a brine solution was carried out following Czerny et al. (2013), yielding an estimated average volume of ~61.6 ± 1.9 m^3 in the mesocosms.

95 All water column manipulations in the mesocosms were achieved with the use of a pumped injection device equipped with polycarbonate piping of various lengths (Riebesell et al., 2013), that was lowered and raised several times in each mesocosm during manipulations to ensure homogeneous distribution throughout the entire water column.

2.2 OAE manipulation

The alkalinity manipulation was performed on day 6 by addition of a sodium hydroxide (NaOH, Merck) solution. To

100 simulate the use of the two alkaline feedstocks: hydrated lime ($Ca(OH)_2$) and olivine (as forsterite, Mg_2SiO_4), NaOH additions were followed by the addition of respective Ca^{2+} and Mg^{2+} rich solutions. These two solutions were prepared using reagent grade calcium chloride ($CaCl_2$) and magnesium chloride ($MgCl_2$). Furthermore, to simulate the release of SiO_3^{2-}, under the olivine scenario, a Si-rich solution was prepared using Na_2SiO_3 (Roth) and added in equal concentrations to all Si-treatments (75 µmol/L), regardless of the targeted alkalinity increase (more details can be found in (Goldenberg

105 et al., 2024). The reasoning behind this decision was to avoid colloid formation that occurs at high Si concentrations (up to 150 µmol/L would have to be added to the highest TA treatment to match the TA to silicate ratio of 4:1 in olivine), and to allow separating between silicate and TA effects. All solutions were prepared by dissolving the corresponding salts in 20L deionized water (Milli-Q®, 18.2 ΩM). Each salt was weighed and dissolved separately. In summary, stock solutions of NaOH and $CaCl_2$ were added to the Ca-based treatments, and $MgCl_2$, NaOH and Na_2SiO_3 to the Si-based ones (the

110 unavoidable increase of TA by adding silicate in the control and ΔTA 150 µmol kg^{-1} was compensated for by adding HCl and not adding NaOH respectively).

2.3 N₂O spiking and nutrient addition

For air-sea gas exchange determination, nitrous oxide (N_2O) additions were performed on day 14 following the procedure described in Czerny et al. (2013). One liter of a saturated stock solution was prepared by bubbling 0.2 μm filtered seawater for two days with N_2O (Nippon Gases). The amounts of stock solution to be added in each mesocosm were calculated using solubility constants by Weiss & Price (1980) and taking into consideration in situ salinities, temperatures and individual mesocosm volumes. The stock solution was then diluted with filtered seawater into 25 L carboys and each mesocosm was spiked with one carboy.

Given the duration of the experiment and the low levels of inorganic nutrients in comparison to the surrounding coastal water, a nutrient addition was performed on day 26. Nitrate concentrations (NO_3^-) were targeted at 4 μmol L^{-1} and phosphate concentrations (PO_4^{3-}) were enhanced following the N:P Redfield ratio of 16:1 (Redfield, 1934).

Ca treatments also received a minor silicate ($Si(OH)_4$) addition in a N:Si ratio of 4:1 to better mimic the natural conditions, without creating a Si-enrichment scenario. Nutrient concentrations were measured the day before nutrient addition and ~2 hours after for quantification and to ensure targeted stoichiometry. It was then noted that the stoichiometry was not even across mesocosms due to underestimated nitrate additions. A successful nitrate amendment was performed on day 28.

2.4 Sampling procedures and CTD operations

Following the alkalinity manipulation, randomized sampling was carried out every second day in the morning hours (08:00 – 12:00). Depth-integrated (0-20m) water samples were taken from the mesocosms and the surrounding coastal water (later referred to as "Fjord") using a 5 L integrating water sampler (IWS, HYDRO-BIOS, Kiel).

Samples were collected in decreasing order of sensitivity to gas exchange, i.e., N_2O, followed by carbonate chemistry and inorganic nutrients. N_2O samples were drawn with a Tygon tube from the IWS directly into 20mL caramel vials in triplicates. After making sure vials were bubble-free, they were crimp sealed immediately and kept at room temperature after fixation with 10 μL of a saturated mercury chloride solution ($HgCl_2$). To minimize gas exchange during air transport and storage, two paraffin wax coats were applied to the crimp seals (Glatzel and Well, 2008; Kock et al., 2016). For carbonate chemistry parameters, such as pH and TA, 0.5 L of seawater were taken into air-tight glass flasks. Clean bottles were pre-rinsed with sample water immediately prior to filling (using pre-rinsed Tygon tubing). Finally, to minimize air–water gas exchange, filling was done gently from bottom to top with an overflow of ~1.5 times the sampling volume (Dickson et al., 2007).

Nutrient subsamples were collected next into 250 mL acid cleaned polypropylene bottles. All samples were kept in cool conditions and protected from direct sunlight until further analysis. Subsamples for NO_3^-, NO_2^-, PO_4^{3-}, and $Si(OH)_4$ were filtered using a PES syringe filter (0.45 μm Sterivex, Merck) and analyzed spectrophotometrically following Hansen and Koroleff (1999).

CTD casts were performed with a multiparameter logging probe (CTD60M, Sea & Sun Technology) directly after the main sampling (14:00 - 16:00), yielding depth profiles of salinity, temperature and pH.

2.5 Sample Analysis

2.5.1 Carbonate Chemistry

All carbonate chemistry analyses were performed in the same way, starting by sterile-filtering the seawater samples through 0.2 μm syringe filters (Sartorius) using Tygon tubing connected to a peristaltic pump. The filtration process resulted in the removal of biomass and potential alkaline particles that may cause changes to seawater carbonate chemistry during analysis (Bockmon and Dickson, 2014). Water for gas-sensitive parameters was subsampled first with gentle flow

and providing an overflow ~1.5 times the final sampling volume. Samples were then kept at room temperature and measured within 12h.

TA was measured by open-cell potentiometric titration as described in Dickson et al. (2007). A 0.05M HCl solution with

155 an ionic strength of 0.72 mol kg^{-1} (corresponding to a salinity of 35 and adjusted by NaCl addition), was used as the titrant. Titrations were performed using a Metrohm Aquatrode Plus (Pt1000) connected to a 907 Titrando, with samples loaded onto an 862 Compact Titrosampler. The temperature was recorded during titration and varied between 20 and 25 °C, i.e., laboratory ambient temperature. 50 g of sample water were weighed into the titration beakers with a precision of 0.1 mg. For every run, results were corrected against certified reference material (CRM, batch 193, Dickson, 2010).

160 Finally, TA was calculated using the titration curves and the "Calkulate" script within PyCO2SYS by (Humphreys et al., 2022). Each sample was measured in duplicate, and the corresponding average and standard deviations are reported. The TA measurement precision was calculated by error propagation of the samples and CRM standard deviations and averaged ±1.9 μmol kg^{-1}.

Seawater pH on the total scale (pH$_T$) was determined spectrophotometrically with a VARIAN Cary 100 in a 10 cm ther-

165 mostated cuvette at 25°C using cresol purple as described in Dickson et al. (2007). Before measurement, samples were acclimated to 25°C in a thermostated water bath. To minimize potential CO_2 air–water gas exchange, a syringe pump (Tecan Cavro XLP) was used for sample and dye mixing and for cuvette injection (see Schulz et al. (2017)). A more detailed description of pH$_T$ corrections is found in Section 2.6.3. The average pH$_T$ precision was estimated at ±0.003 units.

170 DIC samples were taken only on day 9 of the experiment to cross-check the estimated DIC derived from TA and pH$_T$ measurements. Said samples were fixed with $HgCl_2$ for later analysis, conducted on an Automated Infra-Red Inorganic Carbon Analyzer (AIRICA, Marianda), connected to a LI-COR LI-7000 (Gafar and Schulz, 2018). The samples were analyzed in triplicates, and the instrument uncertainty was estimated at ± 1.5 μmol.kg^{-1}.

2.5.2 N$_2$O

175 Aquatic N$_2$O concentrations were measured via gas chromatography (GC) with electron capture detection (ECD) (Hewlett Packard 5890 II), using a headspace static equilibration procedure (precision of ±1.8 %). The GC was equipped with a 6'/1/8'' stainless steel column packed with a 5Å molecular sieve (W. R. Grace & CO) and operated at a constant oven temperature of 190 °C using a 95/5 argon-methane mixture (5.0, AirLiquide) as carrier gas. A 10 mL headspace was manually created in each sample vial with helium (5.0, AirLiquide), and the overflowing water was collected with a

180 second syringe. Next, the vials were shaken vigorously for 20s and left to settle for 2 hours at room temperature. Subsamples of the equilibrated headspace were then injected into the sample loop of the GC. Certified gas mixtures of N$_2$O in artificial air (Deuste Steininger GmbH) with mixing ratios of 330 ± 0.2 and 994 ± 0.2 ppb as well as 6:3 and 4:5 dilutions with helium were used to construct daily calibration curves with a minimum of three data points within the sample concentration range.

185 N$_2$O concentrations were calculated according to Walter et al. (2006) using the solubility function of (Weiss and Price, (1980). The average precision, calculated as mean standard deviation from triplicate measurements, was 0.7 nM.

2.6 Data Analysis

The 53-day experiment was divided into three distinct phases. The pre-treatment phase (day 1 to 6), from here on referred to as phase 0 for simplicity, denotes the baseline state of the system before any alkalinity manipulation. This preliminary

190 phase was an important step to confirm that the starting conditions in all mesocosms were similar. The reaction phase after OAE manipulation (days 7 to 28), phase I, corresponds to the period in-between alkalinity manipulation and the addition of dissolved inorganic nutrients. This post-treatment and pre-fertilization phase mainly consisted of the

immediate response of the system to an increase in alkalinity levels in a post-bloom scenario. The last phase after nutrient addition is referred to as phase II. This post-fertilization period (days 29 to 53) is thought to capture the mid-term indirect responses to alkalinity addition of a biologically active ecosystem state.

Throughout the experiment, two carbonate chemistry parameters (TA and pH_T) were measured and coupled to the corresponding salinity and temperature measurements (daily averages from CTD casts), and nutrient concentrations so the remaining variables of the carbonate system could be calculated (such as DIC, Ω_{Ar} and pCO_2). To do so, the software PyCO2SYS version 1.8.2 (Humphreys et al., 2024) was used with chosen constants for calculations as follows: K1 and K2 for carbonic acid from (Sulpis et al., 2020), $KHSO_4$ from (Dickson, 1990), KHF from (Dickson and Riley, 1979), $[B]_T$ from Uppström, (1974)and the universal gas constant R.

2.6.1 CO₂ fluxes and net community production estimates

To calculate the daily air-sea CO_2 fluxes, N_2O was used as a tracer following the approach described by Czerny et al. (2013) and using measured N_2O to derive transfer velocities (Fig. S3). Fluxes across the water surface (F_{N_2O}) were then calculated as follows:

$$F_{N_2O} = \frac{I_{w1} - I_{w2}}{A * \Delta t} , (1)$$

where I_{w1} and I_{w2} are the fitted bulk water N_2O inventories at time t_1 and t_2, respectively; A is the surface area of the mesocosms; and Δt is the time difference between t_1 and t_2. From here, first N_2O, and then CO_2 transfer velocities were calculated (see Czerny et al. (2013) for details, and note the typo in there, where for the calculation of chemical enhancement the boundary thickness layer z should read 0.02 cm), as shown in Eq. (2), which then allowed to estimate daily CO_2 fluxes (F_{CO2}), according to Eq. (3).

$$k_{CO_2} = \frac{k_{N_2O}}{\sqrt{\frac{Sc_{CO_2}}{Sc_{N_2O}}}} , (2)$$

$$F_{CO_2} = k_{CO_2} * \left(C_{CO_2w} - C_{CO_2weq} \right) , (3)$$

where k_{CO_2} is the transfer velocity of CO_2, Sc_x are the corresponding Schmidt numbers, and C_{CO2w} and C_{CO2weq} are the bulk-water CO_2 concentration and the calculated equilibrium concentration with the atmosphere, respectively. Atmospheric pCO_2 was estimated at 417 µatm (referenced to late spring 2022; Lan et al., 2025; NOAA/GML). Fluxes in this paper are shown as daily changes (mmol C m^{-2} d^{-1}).

Previous mesocosm experiments (Czerny et al., 2013; Spilling et al., 2016) have already shown how CO_2 fluxes can be greatly affected by chemical enhancement due to hydration reactions of CO_2 and conversion to HCO_3^- and CO_3^{2-} in the boundary layer, particularly under low turbulence conditions and high pH (Wanninkhof and Knox, 1996). Given the high concentration of OH^- during this experiment, we applied the correction for chemical enhancement by Hoover and Berkshire (1969) with refitted hydration and hydroxylation rate constants by Schulz et al. (2006). The enhancement factor (α) was calculated following Eq. (4):

$$\alpha = \frac{\tau}{\left[(\tau - 1) + \frac{\tanh(Q * z)}{(Q * z)} \right]} , (4)$$

Where τ represents the chemical enhanced flux and Q (calculated as shown in Czerny et al (2023)) represents the enhanced flux, the hydration of CO_2 and the diffusion coefficient. The average boundary layer thickness z (cm ± std) was calculated to be 0.017 ± 0.003 cm and the overall enhancement ranged from 6% to 20% during this experiment.

2.6.2 Calcification and net community production estimates

235   Cumulative calcification rates (CALC) were estimated following Eq. (5). For this, salinity normalized TA changes (salinity 33 normalized) were calculated, and the uptake of nitrate, i.e., NO_3^-, and phosphate, i.e., PO_4^{3-}, – each of which increases TA by 1 mol per mol of nutrient uptake (Wolf-Gladrow et al., 2007) – was factored in. The cumulative sum of salinity-normalized and nutrient-uptake-corrected TA changes (divided by 2 due to the double contribution of CO_3^{2-} to TA) was then used to gauge overall $CaCO_3$ production in each treatment. Note that the decrease in TA by the uptake of
240   growth-requiring conservative cations such as Mg^{2+}, K^+ and Ca^{2+} (other than that used for calcification) was ignored as being much smaller than the effect of nitrate uptake (Wolf-Gladrow and Klaas, 2024).

$$CALC = -(\Delta TA_{33} + \Delta[NO_3^-]_{33} + \Delta[PO_4^{3-}]_{33}) * 0.5 \ , (5)$$

The $CaCO_3$ production potential (CCPP), i.e., the amount of $CaCO_3$ produced during coccolithophorid bloom (the main
245   calcifier in our experiments), was estimated following Gafar et al. (2018). *In situ* temperature, carbonate chemistry speciation and light conditions at each day for each treatment were considered. Then, normalized CCPP was compared to normalized cumulative $CaCO_3$ production (CALC).

It was also possible to estimate the biologically mediated change of net community production derived from the inorganic carbon fraction (NCP_{DIC}) by accounting for the impact of cumulative CO_2 air-sea exchange (cCO_2) on the cumulative
250   DIC consumption (salinity 33 normalized) and factoring in the formation of $CaCO_3$, as expressed in Eq. (6):

$$NCP_{DIC} = -(\Delta(DIC + cCO_2)_{33} - CALC) \ , (6)$$

Note that cCO_2 is added to DIC in the equation because it has a negative sign by definition. The following change in sign
255   is meant for comparison purposes, since production is often referred to as positive.

2.6.3 pH corrections

Calculations of pH_T included corrections for changes due to dye addition. For that purpose, a batch of sterile filtered seawater (natural seawater filtered through a 0.2 um filter) was prepared and used to achieve 5 different levels of pH by additions of a 1M NaOH solution that would simulate the experimental increments in TA (steps of 0, 150, 300, 450 and
260   600 µmol kg^{-1}). For each level, pH_T was measured for 5 additions of increasing dye addition, and the change in pH_T per addition of dye was calculated. This allowed for the establishment of a calibration curve with a linear correlation between pH_T level and pH_T change due to dye addition (for details see Dickson et al. (2007).

The working range of m-cresol dye has been suggested to be one pH unit below and above the indicator's pK_2 (Hudson-Heck et al., 2021), i.e., about 7-9 at 25°C, which should have covered our experimental range. However, dye impurities
265   can reduce the working range significantly (Schulz et al., 2023). And indeed, we found that above pK_2, there were increasing deviations of measured versus calculated pH_T (from measured DIC and TA on day 9). Hence, a linear correction was applied for those measurements (Fig. S2).

3 Results

3.1 Alkalinity enhancement and carbonate system variability

270　During phase 0, conditions in all mesocosms were relatively similar, averaging 2213 ± 3 µmol kg_{sw}^{-1} for measured TA, 8.109 ± 0.004 for pH_T, 2030 ± 4 µmol kg_{sw}^{-1} for DIC, 339 ± 3 µatm for pCO_2, and 2.00 ± 0.02 for Ω_A (Fig. 1). After the manipulation on day 7, pH_T increased to a maximum of 8.767, and Ω_A up to 7.66 in the two highest treatments, while pCO_2 decreased to 61. In contrast, DIC was hardly affected (Fig. 1 b-e).

Overall, TA remained relatively stable throughout the experiment, regardless of the phase and the treatment (Ca- or Si-
275　based), with a maximum variability of 19 µmol kg^{-1}. Ω_A remained stable throughout Phase I, but showed an increase ranging from ~0.20 to ~0.45 units in each treatment from day 35 onwards (Fig. 1 a, c).

In contrast, changes in pH_T and DIC were observed throughout the experiment. After an initial drop in DIC in all meso-cosms, DIC changes were less consistent over time, with increments of up to 8-28 µmol kg^{-1} in the treatments before the nutrient addition. About a week after the nutrient addition, DIC decreased in all mesocosms again, by about 23-51 µmol
280　kg^{-1}, coinciding with average Chl a changes from 0.53 ± 0.1 µ L^{-1} up to 3.4 ± 0.9 µ L^{-1} during phase II (Fig. S1).
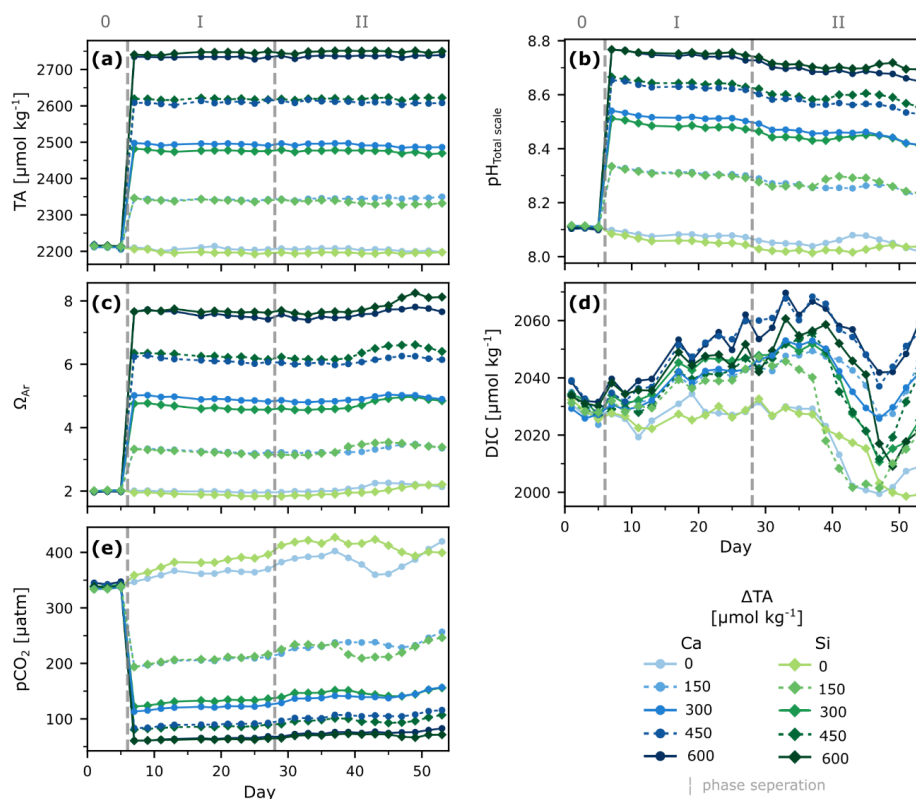

Figure 1: Temporal development of carbonate chemistry parameters under different levels of non-CO₂-equilibrated OAE. Depth-integrated measured TA **(a)**, $pH_{Total scale}$ at in-situ temperatures **(b)**, and calculated aragonite saturation state **(c)**, dissolved inor-
285　ganic carbon **(d)**, and partial pressure of carbon dioxide **(e)**. Dashed lines and roman numbers denote the pre-treatment (0) phase and phases before (I) and after (II) nutrient addition.

3.2 Air-sea CO₂ gas exchange

The experiment began with initial pCO_2 below atmospheric levels, averaging 339 ± 3 µatm across treatments (Fig. 1). All treatments showed an immediate uptake of CO_2, leading to a daily increase in DIC of ~0.1 µmol kg^{-1}. While F_{CO_2} didn't

290 change significantly for the control treatments right after the TA addition, it increased with increasing ΔTA and corresponding lower seawater pCO_2 (Fig. 2). In the highest treatment, F_{CO_2} was five times higher than in the controls. Interestingly, this increasing rate of CO_2 ingassing persisted in all treatments except for the controls, resulting in 50% increase towards the end of the experiment. The total cumulative net uptake of CO_2 ranged from ~16 µmol C kg^{-1} to ~30 µmol C kg^{-1} (see Fig. S4) across treatments. Notably, no differences in F_{CO_2} were observed between the different minerals.
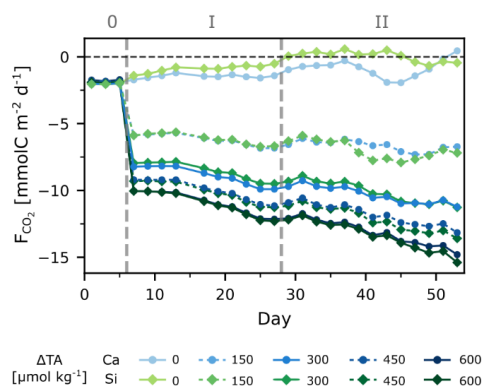
Figure 2: **Daily CO₂ fluxes over time**, with negative values indicating net influx (in-gassing), and positive values net outflux (outgassing) to the atmosphere. See section 2.6.1 for details. Dashed lines and roman numbers denote the different phases.

3.3 Estimated calcification rates and net community production

Except for the Ca-treatment ΔTA 150, the response of normalized cumulative calcification to pCO_2 was that of an opti-

300 mum curve (fitting Eq. 9 from Gafar et al. (2018)), reaching a plateau at about 250 µatm (Fig. 3a). The highest calculated $CaCO_3$ production potential (CCPP) was observed at a pCO_2 of about 200 µatm (Fig. S5). With up to 12 µmol kg^{-1} of $CaCO_3$ produced, cumulative calcification was highest in low-to-intermediate TA treatments and close to zero in the two highest ones (Fig. S4).

NCP_{DIC} showed no significant differences between Si and Ca at the beginning (Fig. 4a). The community reacted to the

305 nutrient addition reaching a peak around 10 to 15 days after it. NCP_{DIC} in the silicate treatments reached about 52 µmolC kg^{-1}, whereas in the calcium treatments the NCP_{DIC} peaks were roughly half in magnitude. To better see potential differences during the bloom phase, we calculated the changes in daily NCP relative to the mean NCP values after nutrient addition and plotted the cumulative changes (Fig. 4b). This gives a clearer perspective of how differently the treatments reacted and the delays in time among blooms, if any, showing as a general trend that silicon-based treatments reached

310 higher bloom peaks than calcium-based ones, and higher alkalinity treatments took longer to start blooming. Though such a statement assumes that the sampling resolution was high enough to capture all real bloom peaks.

To better assess whether a mineral or treatment effect influenced the NCP responses, we proceeded to take maximum production value during the bloom for each treatment and plotted it against the mean pCO_2 value during the bloom period (Fig. 4c). An ANCOVA analysis showed no alkalinity effect, but a clear mineral effect on production.

315
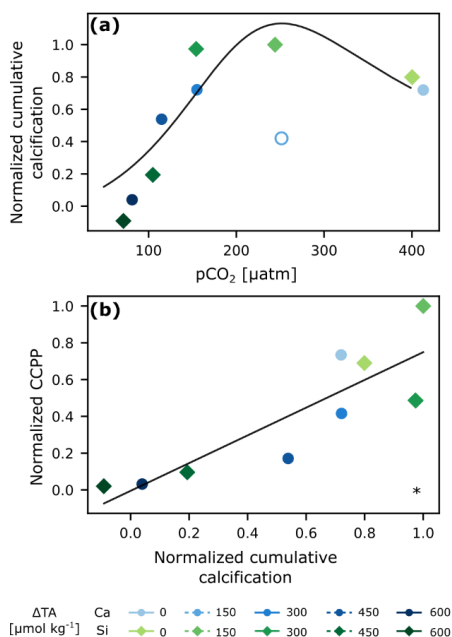
Figure 3: Cumulative calcification (average of last 2 days) derived from carbonate chemistry parameters vs pCO_2 with optimum curve fitting (Eq. 9 in Gafar et al. (2018)) (**a**), and normalized cumulative $CaCO_3$ production potential (CCPP) vs normalized cumulative calcification (**b**). The hollow circle was excluded from analysis. * $p<0.05$
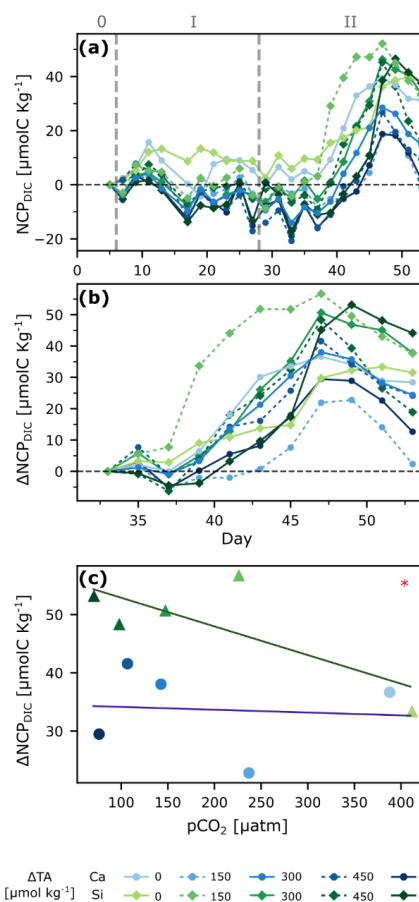
Figure 4: Primary production under OAE. Net community production derived from changes in DIC (NCP_{DIC}, see 2.6.2) over time (**a**), ΔNCP_{DIC} relative to mean after nutrient addition for a better visualization of bloom peaks (**b**), and regression analysis of bloom peaks against pCO_2 levels (**c**). ANCOVA revealed a significant mineral type effect in (**c**): $p<0.05$ (*).

4 Discussion

To decouple air-sea gas exchange from biological DIC drawdown and to investigate the effect of different mineral types, we simulated a non-CO_2-equilibrated deployment of OAE and followed the development of the system over time. Manipulation of total alkalinity resulted in comparable treatment pairs of Ca and Si treatments with the same ΔTA, which remained relatively stable over time. This is most likely because Ω_A did not exceed 11.1, the threshold for spontaneous pseudo-homogeneous carbonate formation in mineral particle-free seawater based on

calculations from Marion et al. (2009) at average salinity of 32.6 and 11°C. Further, the TA manipulation led to expected changes in carbonate chemistry speciation, i.e., increased pH and Ω_A, and decreased pCO_2, plus no

340 significant change to DIC (Fig. 1). In the control treatments, DIC declined slightly during the first 10 days, while staying relatively stable thereafter. In contrast to the stable TA, all manipulated treatments increased their DIC content during phase I. DIC drawdown only began in phase II, about 8 days after the nutrient addition. Changes in DIC ranged from about 23 to 49, in contrast to expected Redfield C:N of 20 (6.625*N). Higher values are normally related to carbon overconsumption, which is known to happen in nutrient limited environments and with

345 increasing temperature (Paul et al., 2016; Taucher et al., 2012). During the bloom in the second phase, pH increases correlate with DIC decreases, suggesting a biological origin, i.e., primary production accompanied by nutrient uptake. Nevertheless, CO_2 uptake from air-sea gas exchange needs to be considered as well before drawing further conclusions.

4.1 Gas exchange

350 F_{CO2} started at about -2 mmol m^2 d^{-1}, indicating that the system was already ingassing CO_2 from the atmosphere. This is related to the fact that we arrived at the study site during in a post-bloom period, i.e., seawater pCO_2 was lower than atmospheric levels, and the concentrations of dissolved inorganic nutrients was low. After alkalinity addition, daily rates increased between ~ 6 mmol m^2 d^{-1} in the lowest treatments and ~-10 mmol m^2 d^{-1} in the higher treatments (Fig. 2), which is within the range of air-sea flux estimates from the region (Aalto et al., 2021).

355 The rates of daily ingassing continued to increase over time, even though the gradient between the atmosphere and seawater pCO_2 would gradually decrease with atmospheric CO_2 uptake. Since the Schmidt number and the viscosity of gases are influenced by temperature, this is a relevant factor when it comes to diffusion of gases, which in this case may have played a major role. Throughout the experiment, temperature increased from ~8.5 to ~15.5 as we moved from late spring to early summer conditions (Fig. S1). Indeed, there was a statistically signif-

360 icant positive correlation of temperature and transfer velocity, and a fitting equation was derived to calculate transfer velocities [cm s^{-1}] from *in situ* temperature [°C] (Eq. 7). We note that while salinity is also an important factor impacting gas exchange, however, due to the relatively small changes throughout our experiment (~0.1 units), the magnitude of the effect was deemed not-significant for the fitting:

365 $$k_{CO_2} = -2.67e^{-4} + 9.61e^{-5} * T_{water} \quad (7)$$

In contrast to a mesocosm setup, the most important factor influencing transfer velocity in open ocean settings is wind speed (v). Though it is widely used to parameterize k_{CO_2}, it has an uncertainty of ~20% and is valid only for wind speeds in the range of 3 to 15 m s^{-1} (Wanninkhof, 2014). To investigate further, we estimated the wind speed

370 according to Wanninkhof (1992) and Wanninkhof et al. (2009) using our derived transfer velocities. At our lowest measured temperature, v was 1.16 m s^{-1}, and, at our highest temperature, 1.92 m s^{-1}. Furthermore, the mean v obtained (at mean salinity and temperature) was 1.49 m s^{-1}, differing from the mean wind speed near the area of about 3.5 m s^{-1} (Weather Underground: Weather data for IHORDALA29, 2025) This is consistent with the use of the mesocosms, which provide some shelter to the enclosed waters in contrast to the surrounding fjord water,

375 reflecting that wind speed alone does not drive gas exchange at low wind, but rather alters water surface texture.

In this regard, Eq. 7 would be more suitable than wind speed to estimate k_{CO_2} under similar conditions, i.e., mesocosm setup and similar ranges of temperature and salinity.

Also interesting is that we reached daily rates of F_{CO_2} up to -15 mmol m^2 d^{-1} for the highest treatments, which equaled to ~30 µmol C kg^{-1} after a period of 47 days for a volume of 61.6 m^3 (20m mixed layer depth). Considering windspeeds of ~1.5 m s^{-1} and a temperature of ~15.5 °C, we simulated further ingassing until full equilibration (95%) of the mixed layer. We found it would take up to ~1050 days to equilibrate. This timeframe is in line with the findings of He & Tyka (2023), who showed most locations to have an uptake efficiency plateau of 0.6–0.8 molCO$_2$ per mol of alkalinity after 3–4 years.

Therefore, our results indicate that seasons should also be considered, at least in models, for possible deployment sites, since temperature is an important driver of the exchange process. Thus, in very cold waters there will likely be slower transfer velocities, not forgetting that windspeed and mixed layer depth would also impact equilibration. Lastly, by accounting for the measured air-sea gas exchange, and factoring in the reductions caused by calcification, it is possible to isolate the change in DIC driven exclusively caused by biological activity such as photosynthesis, and respiration.

4.2 Calcification

Because of the presence of the coccolithophore *E. huxleyi*, and some availability of inorganic nutrients right at the start of the experiment, there was an initial burst of calcification, identified by a concomitant decrease in salinity-normalized TA, which was then quickly ceased due to nutrient limitation. After the addition of nutrients in phase II, calcification increased again, more pronounced in the lower TA treatments and controls (Fig. S4). When overall cumulative calcification is related to pCO$_2$ (Fig. 3), we find an optimum curve as predicted in other lab studies for this CO$_2$ range (Gafar et al., 2018). We see then that mild alkalinity treatments (< ΔTA 300 µmol kg^{-1}) enhanced calcification, while it was reduced and inhibited at ΔTA 450 and 600 µmol kg^{-1} respectively (pCO$_2$ <100 µatm tested here), this falls within the range of mean sensitivity responses to pCO$_2$ for coccolithophores reported by Seifert et al. (2022). Intermediate pCO$_2$ levels seem to provide an optimal balance of bicarbonate ions and H$^+$ concentration, enhancing calcification rates. Both Krug et al. (2011) and Bach et al. (2011) hypothesized that inhibition of calcification could be the result of substrate (CO$_2$ and HCO$_3^-$) limitation on the one hand, and pH/H$^+$ inhibition on the other. The reason for external H$^+$ constituting an inhibitor is that, during coccolithophoride calcification, H$^+$ is internally being generated (e.g., Gafar et al. (2019); Suffrian et al. (2011); Taylor et al. (2011) and eventually needs to be channeled out of the cell to maintain pH homeostasis (Cyronak et al., 2016). Concerning substrate limitation for both calcification and photosynthesis, it does not matter which carbon species is actually being taken up into the cell as at decreasing seawater pCO$_2$, CO$_2$ leakage out of the cytosol (pH ~7, Anning et al. (1996) will increase due to the concentration gradient. Up to a certain level, this could be compensated for by boosting carbon concentration mechanisms such as active CO$_2$ or HCO$_3^-$ uptake, but this would come at increased metabolic costs (Badger and Price, 2003; Reinfelder, 2011).

Additionally, when cumulative TA-based calcification is compared to cumulative coccolithophore abundance (based on flow-cytometric analysis), there is a linear, statistically significant relationship, supporting the assumption of uniform calcification rates across the coccolithophore population (Fig. S5). There is one treatment (Ca 150) that behaves as an outlier though.

While the cumulative calcification calculated here encompasses overall coccolithophore bloom dynamics, the response of calcification to changes in carbonate chemistry are typically described by changes in cellular rates. However, it is possible to link both by calculating the amount of $CaCO_3$ that would be produced in a coccolitho-phore bloom using rates, derived from lab experiments, termed the $CaCO_3$ production potential (CCPP, Gafar et al. (2018). Using the rates collected by Gafar and Schulz (2018) for the coccolithophore *E. huxleyi*, which are dependent on carbonate chemistry, light and temperature, and our average *in-situ* conditions, it is possible to estimate normalized CCPP and compare it to normalized cumulative calcification (Fig. 3b). Here we see a statistically significant linear correlation, suggesting that the overall bloom dynamics derived from changes in measured carbonate chemistry align with the behavior at the cellular level derived independently from rates specific to the coccolithophore *E. huxleyi*. In summary, there is enhanced calcification and CCPP at intermediate levels of pCO_2 (~250 μatm) following a non-CO_2-equilibrated addition of alkalinity, which are negatively impacted when going towards lower and higher levels of pCO_2.

4.3 Net community production as a balance of photosynthesis and respiration

The *in situ* NCP_{DIC} derived from cumulative changes in the DIC pool (Fig. 4) encompasses autotrophic photosynthesis, decreasing DIC through the consumption of CO_2/HCO_3^-, and increasing DIC by both autotrophic and heterotrophic respiration. An increase in photosynthetic activity can be observed after the nutrient addition during phase II, as NCP_{DIC} reached peak values, corroborated by the increase in Chl a (Fig. S1 f). Furthermore, there appeared to be a general trend of silicon-based treatments reaching higher levels of NCP_{DIC} than the calcium-based ones (Fig. 4 c). This may be linked to the stoichiometry of inorganic nutrient availability. While in both treatments' nitrogen uptake was ~3.6 μM, in the silicate treatments, silicate and nitrogen were consumed in a ratio of up to ~3:1. In contrast, in the calcium treatments, the uptake ratio was reversed at ~1:3, meaning that up to ~10 times more silicate was drawn down in the silicate treatments within 20 days. Since the uptake ratio was 10 times higher in Si-treatments generally independently of the TA level, it was likely diatoms (if not in quantity, in frustule thickness) that were heavily silicified, promoting silicification and potential changes to diatom community composition, as discussed by Ferderer et al. (2024). Thus, this suggests that diatoms could allocate additional resources to growth and photosynthesis (Inomura et al., 2023), potentially explaining the higher measured NCP rates (Marín-Samper et al., 2024) in the silicate treatments and, in turn, contributing to the mineral effect detected here on NCP_{DIC}. In summary, it appears that while there was no negative effect of the TA level on NCP_{DIC}, there was a positive effect of the silicate amendment. This is in line with the hypothesis of the *green* ocean suggested by Bach et al. (2019), though the *white* ocean enhanced by added calcium was not observed here. One reason could be low abundances of coccolithophores at the onset of the experiment, the other the fact that increased calcium concentrations paired with increased DIC upon equilibration have been hypothesized to promote coccolithophorid calcification and growth (compare Bach, 2015; Bach et al., 2019). However, given the relatively slow air-sea gas exchange on the order of years and the fact that during this time the TA treated waters are likely subject to substantial dilution (significantly reducing TA and hence the DIC increase upon full equilibration), a white ocean might not be something to expect.

The delay in bloom formation observed here (Fig. 4b) was also reflected in *in vitro* oxygen production rates (Marín-Samper et al., 2024) and was related to both the mineral treatment and the TA level. These delays can be attributed to the previously reported, species-specific negative relationships between elevated pH/ low pCO_2 levels

and phytoplankton growth rates (Chen and Durbin, 1994; Hansen, 2002), as well as the substrate/inhibitor concept already mentioned above. However, in terms of ecological significance, it is not clear if a phytoplankton bloom

455 delay causes knock-on effects for higher trophic levels. Hence, at this stage, it is difficult to draw clear conclusions or provide recommendations.

4.4 Zooplankton respiration

The main difference between the estimated *in situ* NCP_{DIC} and NCP obtained from O_2 measurements in separate incubations is the exclusion of grazers (larger than 280 μm) in the latter since samples are screened before incu-

460 bation. So, when comparing both, it is possible to get an estimation of the contribution of larger zooplankton and fish respiration to the carbon balance (Eq. 8):

$$RZ = NCP - NCP_{DIC} \text{ , (8)}$$

465 with RZ denoting zooplankton respiration and NCP the cumulative net community production derived from O_2 incubation measurements, assuming a 1:1 O_2:C conversion ratio. Cumulative RZ ranged from 30-60 μmol kg^{-1} and was significantly correlated to pCO_2 as well as to mineral treatment (Fig. 5). Interestingly, the treatments with lower NCP_{DIC} had higher RZ, possibly indicating a top-down control on primary productivity. Reasons for this observation could be direct effects of high pH at low pCO_2 on zooplankton metabolism (Hessen and Nilssen, 1983;

470 Pedersen and Hansen, 2003), if requiring more energy along the TA gradient to maintain homeostasis under suboptimal conditions, or indicating effects of changes to phytoplankton community composition, influencing prey availability between the two mineral types. Furthermore, under low pCO_2 conditions, phytoplankton have lower C:N content (Burkhardt et al., 1999), which increases their quality as food for zooplankton, likely leading to higher grazing and respiration rates. All this suggests that the response to carbonate chemistry perturbations

475 might also be species-specific and that a top-down control on primary productivity might have been exerted. Interestingly, Goldenberg et al. (2024) showed that though fish abundance in our experiment did not correlate to the treatment gradient, biomass did. Although no clear explanation could be found by the authors, it highlights the complex trophic interactions in pelagic ecosystems that require untangling. Finally, a recent study showed enhanced copepod grazing rates for certain OAE scenarios, although respiration rates didn't seem to be correlated

480 (Bhaumik et al., 2025), again highlighting the lack of mechanistic understanding of the underlying processes.
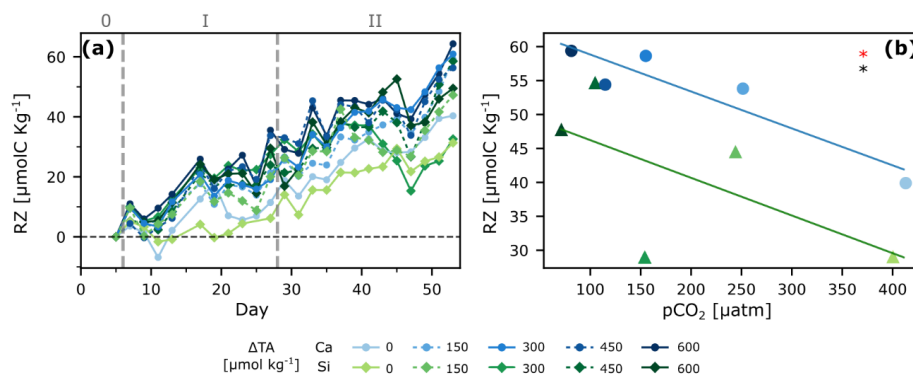
Figure 5: Zooplankton under OAE. Respiration of Zooplankton (RZ) over time (**a**), and regression analysis of the last 2 days (averaged) vs pCO_2 (**b**). ANCOVA results: OAE (treatment) effect: $p < 0.05$(*), and mineral type effect: $p < 0.05$(*).

485

Table 1: Summary of responses under non-CO_2-equilibrated OAE. "**=**" indicates no effect detected, while "**✓**" indicates a detected effect. The arrows depict the direction of the response to the TA gradient (decreased, ↓; enhanced, ↑).

Response variable	Mineral type effect	OAE effect	Remarks
CO_2 ingassing	=	↑	Increased with decreasing pCO_2 Up to 15 mmolC m^{-2} d^{-1}
Coccolithophorid Calcification	=	*↓	*Optimum curve response, peaking at ΔTA 150 µmol kg^{-1} and pCO_2 ~250 µatm, then decreasing
Net Community Production	✓	=	More pronounced in Si treatments
Zooplankton Respiration	✓	↑	Higher in Ca treatments Increased with lower pCO_2

5 Conclusions and outlook

490

Our study shows that CO_2 ingassing can occur at rates of up to 15 mmol C m^{-2} per day after a non-CO_2-equilibrated deployment of OAE. This equates to ~30 µmol C kg^{-1} over 47 days for a 61.6 m³ volume under low wind conditions, reaching full equilibration after ~1050 days. Furthermore, phytoplankton responses showed an optimum curve for coccolithophorid calcification with peaks at mild treatments (TA 150 µmol kg^{-1}, pCO_2 ~250 µatm),

495

aligning with previous laboratory predictions. No significant effect on NCP_{DIC} was observed with lowered pCO_2, but a mineral effect was noted, with maximum NCP_{DIC} being more pronounced in Si treatments, potentially due to enhanced $Si(OH)_4$ concentrations. Lastly, zooplankton respiration was lower in silicate treatments and increased with lower pCO_2, indicating species-specific responses and potential top-down control on primary productivity. Based on our findings (Table 1), we conclude that under a scenario without coinciding silicate addition, an OAE

500 application would be unlikely to have a significant impact on the plankton community up to levels around ΔTA of 150 μmol kg^{-1}. At higher TA levels, in particular in conjunction with added silicate, there might be complex interactions among multiple trophic levels, requiring further disentangling.

Data availability

All data supporting this article will be available for open access on the PANGAEA data portal upon publication.

505 **Supplement link**

(to be added by Copernicus)

Figure S1: Temporal development of environmental conditions

Figure S2: pH correction/calibration

Figure S3: N$_2$O measured concentrations and chemical enhancement

510 Figure S4: Net community production related figures

Figure S5: Calcification related figures

Author contribution statement

UR, KGS and LRK designed and conceptualized the mesocosm experiment. JS, KGS, CAM, LMS, LRK and JOC collected and analyzed samples in the laboratory. JS and KGS were responsible for data curation and formal

515 analysis. JS, KGS, CAM and LMS interpreted results. JS prepared the original draft with particular input from KGS and contributions from all co-authors.

Competing interests

The research reported in the manuscript was conducted during academic activities, prior to the start of other employment. Julieta Schneider has been consulting for the start-up Planeteers GmbH, Germany, as a Geochemical

520 Researcher since November 2024, and Joaquín Ortíz-Cortes is employed by Macrocarbon S.L., Spain, since October 2023.

References

Aalto, N. J., Campbell, K., Eilertsen, H. C., and Bernstein, H. C.: Drivers of Atmosphere-Ocean CO2 Flux in Northern Norwegian Fjords, Front Mar Sci, 8, 692093, https://doi.org/10.3389/FMARS.2021.692093, 2021.

Anning, T., Nimer, N., Merrett, M. J., and Brownlee, C.: Costs and benefits of calcification in coccolithophorids,

545 Journal of Marine Systems, 9, 45–56, https://doi.org/10.1016/0924-7963(96)00015-2, 1996.

Weather Underground: Weather data for IHORDALA29: https://www.wunderground.com/dashboard/pws/IHORDALA29/graph/2022-07-20/2022-07-20/monthly, last access: 30 January 2025.

Bach, L. T.: Reconsidering the role of carbonate ion concentration in calcification by marine organisms, Biogeosciences, 12, 4939–4951, https://doi.org/10.5194/BG-12-4939-2015, 2015.

550 Bach, L. T., Riebesell, U., and Schulz, K. G.: Distinguishing between the effects of ocean acidification and ocean carbonation in the coccolithophore Emiliania huxleyi, Limnol Oceanogr, 56, 2040–2050, https://doi.org/10.4319/lo.2011.56.6.2040, 2011.

Bach, L. T., Gill, S. J., Rickaby, R. E. M., Gore, S., and Renforth, P.: CO2 Removal With Enhanced Weathering and Ocean Alkalinity Enhancement: Potential Risks and Co-benefits for Marine Pelagic Ecosystems, Frontiers in

555 Climate, 1, 7, https://doi.org/10.3389/fclim.2019.00007, 2019.

Badger, M. R. and Price, G. D.: CO2 concentrating mechanisms in cyanobacteria: molecular components, their diversity and evolution, J Exp Bot, 54, 609–622, https://doi.org/10.1093/jxb/erg076, 2003.

Bhaumik, A., Faucher, G., Henning, M., Meunier, C. L., and Boersma, M.: Prey dynamics as a buffer: Enhancing copepod resilience to Ocean Alkalinity Enhancement, Environmental Research Letters,

560 https://doi.org/10.1088/1748-9326/adaa8c, 2025.

Bockmon, E. E. and Dickson, A. G.: A seawater filtration method suitable for total dissolved inorganic carbon and pH analyses, Limnol Oceanogr Methods, 12, 191–195, https://doi.org/10.4319/LOM.2014.12.191, 2014.

Burkhardt, S., Zondervan, I., and Riebesell, U.: Effect of CO2 concentration on C:N:P ratio in marine phytoplankton: A species comparison, Limnol Oceanogr, 44, 683–690, https://doi.org/10.4319/lo.1999.44.3.0683, 1999.

565 Caserini, S., Pagano, D., Campo, F., Abbà, A., De Marco, S., Righi, D., Renforth, P., and Grosso, M.: Potential of Maritime Transport for Ocean Liming and Atmospheric CO2 Removal, Frontiers in Climate, 3, 1–18, https://doi.org/10.3389/fclim.2021.575900, 2021.

Chen, C. Y. and Durbin, E. G.: Effects of pH on the growth and carbon uptake of marine phytoplankton, Mar Ecol Prog Ser, 109, 83–94, https://doi.org/10.3354/meps109083, 1994.

570 Cyronak, T., Schulz, K. G., and Jokiel, P. L.: The Omega myth: what really drives lower calcification rates in an acidifying ocean, ICES Journal of Marine Science, 73, 558–562, https://doi.org/10.1093/ICESJMS/FSV075, 2016.

Czerny, J., Schulz, K. G., Ludwig, A., and Riebesell, U.: Technical Note: A simple method for air-sea gas exchange measurements in mesocosms and its application in carbon budgeting, Biogeosciences, 10, 1379–1390,

575 https://doi.org/10.5194/bg-10-1379-2013, 2013.

Denman, K. L.: Climate change, ocean processes and ocean iron fertilization, Mar Ecol Prog Ser, 364, 219–225, https://doi.org/10.3354/meps07542, 2008.

Dickson, A. G.: Thermodynamics of the dissociation of boric acid in synthetic seawater from 273.15 to 318.15 K, Deep Sea Research Part A. Oceanographic Research Papers, 37, 755–766, https://doi.org/10.1016/0198-

580 0149(90)90004-F, 1990.

Dickson, A. G.: Standards for Ocean Measurements, Oceanography, 23, 34–47, https://doi.org/10.5670/OCEANOG.2010.22, 2010.

Dickson, A. G. and Riley, J. P.: The estimation of acid dissociation constants in sea-water media from potentiometric titrations with strong base. II. The dissociation of phosphoric acid, Mar Chem, 7, 101–109, 585 https://doi.org/10.1016/0304-4203(79)90002-1, 1979.

Dickson, A. G., Sabine, C. L., and Christian, J. R.: Guide to best practices for ocean CO_2 measurements, North Pacific Marine Science Organization, 191 pp., 2007.

Doney, S. C., Shallin Busch, D., Cooley, S. R., and Kroeker, K. J.: The Impacts of Ocean Acidification on Marine Ecosystems and Reliant Human Communities, Annu Rev Environ Resour, 45, 83–112, https://doi.org/10.1146/an-590 nurev-environ-012320, 2020.

Feng, E. Y., Keller, D. P., Koeve, W., and Oschlies, A.: Could artificial ocean alkalinization protect tropical coral ecosystems from ocean acidification?, Environmental Research Letters, 11, 074008, https://doi.org/10.1088/1748-9326/11/7/074008, 2016.

Ferderer, A., Schulz, K. G., Riebesell, U., Baker, K. G., Chase, Z., and Bach, L. T.: Investigating the effect of 595 silicate-and calcium-based ocean alkalinity enhancement on diatom silicification, Biogeosciences, 21, 2777–2794, https://doi.org/10.5194/bg-21-2777-2024, 2024.

Fuhr, M., Geilert, S., Schmidt, M., Liebetrau, V., Vogt, C., Ledwig, B., and Wallmann, K.: Kinetics of Olivine Weathering in Seawater: An Experimental Study, Frontiers in Climate, 4, 831587, https://doi.org/10.3389/fclim.2022.831587, 2022.

600 Gafar, N. A. and Schulz, K. G.: A three-dimensional niche comparison of Emiliania huxleyi and Gephyrocapsa oceanica: Reconciling observations with projections, Biogeosciences, 15, 3541–3560, https://doi.org/10.5194/BG-15-3541-2018, 2018.

Gafar, N. A., Eyre, B. D., and Schulz, K. G.: A conceptual model for projecting coccolithophorid growth, calcification and photosynthetic carbon fixation rates in response to global ocean change, Front Mar Sci, 4, 605 https://doi.org/10.3389/FMARS.2017.00433, 2018.

Gafar, N. A., Eyre, B. D., and Schulz, K. G.: Particulate inorganic to organic carbon production as a predictor for coccolithophorid sensitivity to ongoing ocean acidification, Limnol Oceanogr Lett, 4, 62–70, https://doi.org/10.1002/LOL2.10105, 2019.

Glatzel, S. and Well, R.: Evaluation of septum-capped vials for storage of gas samples during air transport, Envi-610 ron Monit Assess, 136, 307–311, https://doi.org/10.1007/S10661-007-9686-2, 2008.

Goldenberg, S. U., Riebesell, U., Brüggemann, D., Börner, G., Sswat, M., Folkvord, A., Couret, M., Spjelkavik, S., Sánchez, N., Jaspers, C., and Moyano, M.: Early life stages of fish under ocean alkalinity enhancement in coastal plankton communities, Biogeosciences, 21, 4521–4532, https://doi.org/10.5194/bg-21-4521-2024, 2024.

Hansen, H. P. and Koroleff, F.: Determination of nutrients, in: Methods of Seawater Analysis, John Wiley & Sons, 615 Ltd, 159–228, https://doi.org/10.1002/9783527613984.ch10, 1999.

Hansen, P. J.: Effect of high pH on the growth and survival of marine phytoplankton: implications for species succession, Aquatic Microbial Ecology, 28, 279–288, 2002.

Hartmann, J., West, A. J., Renforth, P., Köhler, P., De La Rocha, C. L., Wolf-Gladrow, D. A., Dürr, H. H., and Scheffran, J.: Enhanced chemical weathering as a geoengineering strategy to reduce atmospheric carbon dioxide,

620   supply   nutrients,   and   mitigate   ocean   acidification,   Reviews   of   Geophysics,   51,   113–149,
        https://doi.org/10.1002/ROG.20004, 2013.

        Hartmann, J., Suitner, N., Lim, C., Schneider, J., Marín-Samper, L., Arístegui, J., Renforth, P., Taucher, J., and
        Riebesell, U.: Stability of alkalinity in ocean alkalinity enhancement (OAE) approaches-consequences for dura-
        bility of CO 2 storage, Biogeosciences, 20, 781–802, https://doi.org/10.5194/bg-20-781-2023, 2023.

625   He, J. and Tyka, M. D.: Limits and CO2 equilibration of near-coast alkalinity enhancement, Biogeosciences, 20,
        27–43, https://doi.org/10.5194/bg-20-27-2023, 2023.

        Henderson, G., Rickaby, R., and Bouman, H.: Decreasing atmosphere CO2 by increasing ocean alkalinity the
        ocean dimension: would the concept work and what would be the environmental consequences? A report based
        on literature sources and simple calculations, University of Oxford, 2008.

630   Hessen, D. O. and Nilssen, J. P.: High pH and the abundances of two commonly co-ocurring freshwater copepods
        (Copepoda, Cyclopida), Ann Limnol, 19, 195–201, https://doi.org/10.1051/limn/1983022, 1983.

        Ho,   D.   T.:   Carbon   dioxide   removal   is   an   ineffective   time   machine,   Nature,   616,   9,
        https://doi.org/10.1038/D41586-023-00953-X, 2023.

        Hoover, T. E. and Berkshire, D. C.: Effects of hydration on carbon dioxide exchange across an air-water interface,
635   J Geophys Res, 74, 456–464, https://doi.org/10.1029/jb074i002p00456, 1969.

        Hudson-Heck, E., Liu, X., and Byrne, R. H.: Purification and Physical−Chemical Characterization of Bromocresol
        Purple for Carbon System Measurements in Freshwaters, Estuaries, and Oceans, ACS Omega, 6, 17941–17951,
        https://doi.org/10.1021/acsomega.1c01579, 2021.

        Humphreys, M. P., Lewis, E. R., Sharp, J. D., and Pierrot, D.: PyCO2SYS v1.8: marine carbonate system calcu-
640   lations in Python, Geosci. Model Dev, 15, 15–43, https://doi.org/10.5194/gmd-15-15-2022, 2022.

        Humphreys, M. P., Schiller, A. J., Sandborn, D., Gregor, L., Pierrot, D., van Heuven, S. M. A. C., Lewis, E. R.,
        and Wallace, D. W. R.: PyCO2SYS: marine carbonate system calculations in Python, https://doi.org/10.5281/ZE-
        NODO.14506565, 2024.

        Inomura, K., José, J., Karlusich, P., Dutkiewicz, S., Deutsch, C., Harrison, P. J., and Bowler, C.: High Growth
645   Rate of Diatoms Explained by Reduced Carbon Requirement and Low Energy Cost of Silica Deposition, Micro-
        biol Spectr, 11, e0331122, https://doi.org/10.1128/SPECTRUM.03311-22, 2023.

        IPCC: Summary for Policymakers, in: Climate Change 2021: The Physical Science Basis. Contribution of Work-
        ing Group I to the Sixth Assessment Report of the Intergovernmental Panel on Climate Change, edited by: Mas-
        son-Delmotte, V., Zhai, P., Pirani, A., Connors, S. L., Péan, C., Berger, S., Caud, N. , C. L., Goldfarb, M. I.,
650   Gomis, M., Huang, K., Leitzell, E. L. J. B. R., Matthews, Y., Maycock, T. K., Waterfield, T., Yelekçi, O., Yu, R.,
        and Zhou, B., Cambridge University Press, Cambridge, https://doi.org/10.1017/9781009157896.001, 2021.

        Kheshgi, H. S.: Sequestering atmospheric carbon dioxide by increasing ocean alkalinity, Energy, 20, 915–922,
        https://doi.org/10.1016/0360-5442(95)00035-F, 1995.

        Kock, A., Arevalo-Martinez, D. L., Loscher, C. R., and Bange, H. W.: Extreme N2O accumulation in the coastal
655   oxygen minimum zone off Peru, Biogeosciences, 13, 827–840, https://doi.org/10.5194/BG-13-827-2016, 2016.

        Köhler, P., Hartmann, J., and Wolf-Gladrow, D. A.: Geoengineering potential of artificially enhanced silicate
        weathering of olivine, Proc Natl Acad Sci U S A, 107, 20228–20233, https://doi.org/10.1073/pnas.1000545107,
        2010.

Kroeker, K. J., Kordas, R. L., Crim, R. N., and Singh, G. G.: Meta-analysis reveals negative yet variable effects
660   of ocean acidification on marine organisms, Ecol Lett, 13, 1419–1434, https://doi.org/10.1111/j.1461-
       0248.2010.01518.x, 2010.

Krug, S. A., Schulz, K. G., and Riebesell, U.: Effects of changes in carbonate chemistry speciation on Coccolithus
       braarudii: A   discussion   of   coccolithophorid   sensitivities,   Biogeosciences,   8,   771–777,
       https://doi.org/10.5194/BG-8-771-2011, 2011.

665   NOAA Global Monitoring Laboratory: Trends in CO2: https://gml.noaa.gov/ccgg/trends/gl_data.html, last ac-
       cess: 20 January 2025.

Marín-Samper, L., Arístegui, J., Hernández-Hernández, N., and Riebesell, U.: Responses of microbial metabolic
       rates to non-equilibrated silicate-versus calcium-based ocean alkalinity enhancement, Biogeosciences, 21, 5707–
       5724, https://doi.org/10.5194/bg-21-5707-2024, 2024.

670   Marion, G. M., Millero, F. J., and Feistel, R.: Salinity/temperature ranges for seawater SA-T-P models, Ocean
       Science, 5, 285–291, https://doi.org/10.5194/OS-5-285-2009, 2009.

Montserrat, F., Renforth, P., Hartmann, J., Leermakers, M., Knops, P., and Meysman, F. J. R.: Olivine Dissolution
       in Seawater: Implications for CO 2 Sequestration through Enhanced Weathering in Coastal Environments,
       https://doi.org/10.1021/acs.est.6b05942, 2017.

675   Moras, C. A., Bach, L. T., Cyronak, T., Joannes-Boyau, R., and Schulz, K. G.: Ocean alkalinity enhancement –
       avoiding runaway CaCO3 precipitation during quick and hydrated lime dissolution, Biogeosciences, 19, 3537–
       3557, https://doi.org/10.5194/bg-19-3537-2022, 2022.

Moras, C. A., Cyronak, T., Bach, L. T., Joannes-Boyau, R., and Schulz, K. G.: Effects of grain size and seawater
       salinity on magnesium hydroxide dissolution and secondary calcium carbonate precipitation kinetics: implications
680   for ocean alkalinity enhancement, Biogeosciences, 21, 3463–3475, https://doi.org/10.5194/bg-21-3463-2024,
       2024.

National Academies of Sciences, E. and M.: A Research Strategy for Ocean-based Carbon Dioxide Removal and
       Sequestration, National Academies Press, Washington DC, 1–308 pp., https://doi.org/10.17226/26278, 2022.

Oschlies, A., Bach, L. T., Rickaby, R. E. M., Satterfield, T., Webb, R., and Gattuso, J.-P.: Climate targets, carbon
685   dioxide removal, and the potential role of ocean alkalinity enhancement, State of the Planet, 2-oae2023, 1–9,
       https://doi.org/10.5194/sp-2-oae2023-1-2023, 2023.

Paul, A. J., Haunost, M., Goldenberg, S. U., Hartmann, J., Sánchez, N., Schneider, J., Suitner, N., and Riebesell,
       U.: Ocean alkalinity enhancement in an open ocean ecosystem: Biogeochemical responses and carbon storage
       durability, EGUsphere [preprint], https://doi.org/10.5194/egusphere-2024-417, 2024.

690   Paul, C., Sommer, U., Garzke, J., Moustaka-Gouni, M., Paul, A., and Matthiessen, B.: Effects of increased CO2
       concentration on nutrient limited coastal summer plankton depend on temperature, Limnol Oceanogr, 61, 853–
       868, https://doi.org/10.1002/LNO.10256, 2016.

Pedersen, M. F. and Hansen, P. J.: Effects of high pH on a natural marine planktonic community, Mar Ecol Prog
       Ser, 260, https://doi.org/10.3354/meps260019, 2003.

695   Peters, G. P.: The "best available science" to inform 1.5 °C policy choices, Nat Clim Chang, 6, 646–649,
       https://doi.org/10.1038/nclimate3000, 2016.

Redfield, A. C.: On the proportions of organic derivatives in sea water and their relation to the composition of
       plankton, University Press of Liverpool, 176–192 pp., 1934.

Reinfelder, J. R.: Carbon concentrating mechanisms in eukaryotic marine phytoplankton, Ann Rev Mar Sci, 3,
700   291–315, https://doi.org/10.1146/ANNUREV-MARINE-120709-142720/CITE/REFWORKS, 2011.

Renforth, P. and Henderson, G.: Assessing ocean alkalinity for carbon sequestration, Reviews of Geophysics, 55,
636–674, https://doi.org/10.1002/2016RG000533, 2017.

Riebesell, U., Czerny, J., von Bröckel, K., Boxhammer, T., Deckelnick, M., Fischer, M., Hoffmann, D., Krug, S.
A., Lentz, U., Ludwig, A., Muche, R., and Schulz, K. G.: Technical Note: A mobile sea-going mesocosm system-
705   new opportunities for ocean change research, Biogeosciences, 10, 1835–1847, https://doi.org/10.5194/bg-10-
1835-2013, 2013.

Rogelj, J., Schaeffer, M., Friedlingstein, P., Gillett, N. P., Van Vuuren, D. P., Riahi, K., Allen, M., and Knutti, R.:
Differences between carbon budget estimates unravelled, https://doi.org/10.1038/nclimate2868, 1 March 2016.

Rogelj, J., Popp, A., Calvin, K. V., Luderer, G., Emmerling, J., Gernaat, D., Fujimori, S., Strefler, J., Hasegawa,
710   T., Marangoni, G., Krey, V., Kriegler, E., Riahi, K., Van Vuuren, D. P., Doelman, J., Drouet, L., Edmonds, J.,
Fricko, O., Harmsen, M., Havlík, P., Humpenöder, F., Stehfest, E., and Tavoni, M.: Scenarios towards limiting
global mean temperature increase below 1.5 °c, Nat Clim Chang, 8, 325–332, https://doi.org/10.1038/s41558-
018-0091-3, 2018.

Sabine, C. L. and Tanhua, T.: Estimation of Anthropogenic CO2 Inventories in the Ocean, Annu. Rev. Marine.
715   Sci, 2, 175–198, https://doi.org/10.1146/annurev-marine-120308-080947, 2010.

Schellnhuber, H. J., Rahmstorf, S., and Winkelmann, R.: Why the right climate target was agreed in Paris, Nat.
Clim. Chang, 6, 649–653, https://doi.org/10.1038/nclimate3013, 2016.

Schulz, K. G., Riebesell, U., Rost, B., Thoms, S., and Zeebe, R. E.: Determination of the rate constants for the
carbon dioxide to bicarbonate inter-conversion in pH-buffered seawater systems, https://doi.org/10.1016/j.mar-
720   chem.2005.11.001, 2006.

Schulz, K. G., Bach, L. T., Bellerby, R. G. J., Bermúdez, R., Büdenbender, J., Boxhammer, T., Czerny, J., Engel,
A., Ludwig, A., Meyerhöfer, M., Larsen, A., Paul, A. J., Sswat, M., and Riebesell, U.: Phytoplankton blooms at
increasing levels of atmospheric carbon dioxide: Experimental evidence for negative effects on prymnesiophytes
and positive on small picoeukaryotes, Front Mar Sci, 4, https://doi.org/10.3389/fmars.2017.00064, 2017.

725   Schulz, K. G., Bach, L. T., and Dickson, A. G.: Seawater carbonate system considerations for ocean alkalinity
enhancement research, State Planet Discuss, https://doi.org/10.5194/sp-2023-12, 2023.

Seifert, M., Nissen, C., Rost, B., and Hauck, J.: Cascading effects augment the direct impact of CO2 on phyto-
plankton growth in a biogeochemical model, Elementa: Science of the Anthropocene, 10,
https://doi.org/10.1525/ELEMENTA.2021.00104, 2022.

730   Spilling, K., Schulz, K. G., Paul, A. J., Boxhammer, T., Achterberg, E. P., Hornick, T., Lischka, S., Stuhr, A.,
Bermúdez, R., Czerny, J., Crawfurd, K., Brussaard, C. P. D., Grossart, H.-P., and Riebesell, U.: Effects of ocean
acidification on pelagic carbon fluxes in a mesocosm experiment, Biogeosciences, 13, 6081–6093,
https://doi.org/10.5194/bg-13-6081-2016, 2016.

Suffrian, K., Schulz, K. G., Gutowska, M. A., Riebesell, U., and Bleich, M.: Cellular pH measurements in Emili-
735   ania huxleyi reveal pronounced membrane proton permeability, New Phytologist, 190, 595–608,
https://doi.org/10.1111/J.1469-8137.2010.03633.X, 2011.

Suitner, N., Faucher, G., Lim, C., Schneider, J., Moras, C. A., Riebesell, U., and Hartmann, J.: Ocean alkalinity
enhancement approaches and the predictability of runaway precipitation processes: results of an experimental

study to determine critical alkalinity ranges for safe and sustainable application scenarios, Biogeosciences, 21,
4587–4604, https://doi.org/10.5194/bg-21-4587-2024, 2024.

Sulpis, O., Lauvset, S. K., and Hagens, M.: Current estimates of K * 1 and K * 2 appear inconsistent with measured
CO_2 system parameters in cold oceanic regions, Ocean Sci, 16, 847–862, https://doi.org/10.5194/os-16-847-
2020, 2020.

Taucher, J., Schulz, K. G., Dittmar, T., Sommer, U., Oschlies, A., and Riebesell, U.: Enhanced carbon overcon-
sumption in response to increasing temperatures during a mesocosm experiment, Biogeosciences, 9, 3531–3545,
https://doi.org/10.5194/bg-9-3531-2012, 2012.

Taylor, A. R., Chrachri, A., Wheeler, G., Goddard, H., and Brownlee, C.: A voltage-gated H+ channel underlying
pH homeostasis in calcifying coccolithophores, PLoS Biol, 9, e1001085, https://doi.org/10.1371/JOUR-
NAL.PBIO.1001085, 2011.

Uppström, L. R.: The boron/chlorinity ratio of deep-sea water from the Pacific Ocean, Deep Sea Research and
Oceanographic Abstracts, 21, 161–162, https://doi.org/10.1016/0011-7471(74)90074-6, 1974.

Van Vuuren, D. P., Stehfest, E., Gernaat, D. E. H. J., Van Den Berg, M., Bijl, D. L., De Boer, H. S., Daioglou,
V., Doelman, J. C., Edelenbosch, O. Y., Harmsen, M., Hof, A. F., and Van Sluisveld, M. A. E.: Alternative path-
ways to the 1.5 °c target reduce the need for negative emission technologies, Nat Clim Chang, 8, 391–397,
https://doi.org/10.1038/s41558-018-0119-8, 2018.

Walter, S., Bange, H. W., Breitenbach, U., and Wallace, D. W. R.: Nitrous oxide in the North Atlantic Ocean,
Biogeosciences, 3, 607–619, 2006.

Wanninkhof, R.: Relationship between wind speed and gas exchange over the ocean, J Geophys Res Oceans, 97,
7373–7382, https://doi.org/10.1029/92JC00188, 1992.

Wanninkhof, R.: Relationship between wind speed and gas exchange over the ocean revisited, Limnol Oceanogr
Methods, 12, 351–362, https://doi.org/10.4319/LOM.2014.12.351, 2014.

Wanninkhof, R. and Knox, M.: Chemical enhancement of CO2 exchange in natural waters, Limnol Oceanogr, 41,
689–697, https://doi.org/10.4319/LO.1996.41.4.0689, 1996.

Wanninkhof, R., Asher, W. E., Ho, D. T., Sweeney, C., and McGillis, W. R.: Advances in quantifying air-sea gas
exchange and environmental forcing, Ann Rev Mar Sci, 1, 213–244, https://doi.org/10.1146/annurev.ma-
rine.010908.163742, 2009.

Weiss, R. F. and Price, B. A.: Nitrous oxide solubility in water and seawater, Mar Chem, 8, 347–359, 1980.

Wolf-Gladrow, D. A. and Klaas, C.: Total alkalinity change: The perspective of phytoplankton stoichiometry,
Limnol Oceanogr, 69, 1900–504, https://doi.org/10.1002/lno.12597, 2024.

Wolf-Gladrow, D. A., Zeebe, R. E., Klaas, C., Körtzinger, A., and Dickson, A. G.: Total alkalinity: The explicit
conservative expression and its application to biogeochemical processes, Mar Chem, 106, 287–300,
https://doi.org/10.1016/j.marchem.2007.01.006, 2007.